Biomedical Research

The research of the institute on the application of radiation and nuclear physics techniques to the fields of biology and medicine concentrates on two topics: Cell radiobiology with quasi-monochromatic X-rays and positron emission tomography (PET) for quality assurance of charged hadron tumour therapy.

While the PET-method is in routine clinical operation at the experimental heavy ion therapy facility at GSI Darmstadt, the radiobiology equipment at the radiation source ELBE is under preparation. The first research activity will be aimed at measurements of the relative biological effectiveness (RBE) for photon energies between 10 and 100 keV. Since such X-rays are widely used in diagnostic radiology (e. g. mammography) and since it has been recently shown by means of soft X-ray tubes that the RBE for cell death as well as for the induction of genomic defects is photon energy dependent, a precise knowledge of these RBE values is highly desirable for radiation protection purposes. Furthermore, these data are relevant for treatment planning in radionuclide or brachytherapy, if isotopes emitting low-energy photons or the recently developed miniature X-ray tubes are applied. In a common project together with the Institute of Bioinorganic and Radiopharmaceutical Chemistry of the FZR the energy dependent increase of the RBE of photons caused by the accumulation of molecules containing atoms of high atomic number within the radiation sensitive structures of the cells will be investigated. The basis for this research are quasi-monochromatic X-rays which will be produced at ELBE by means of channeling relativistic electrons through crystalline matter (diamond). The preparations of radiobiological experiments at ELBE comprised in 2001:

- *the completion of a cell culture laboratory in the ELBE building;*
- *experiments on the determination of RBE of photons from conventional soft X-ray tubes;*
- *on-line dosimetry at well as off-line dose measurements in volumes of subcellular scale;*
- *the design of an X-ray monochromator of highly oriented pyrolythic graphite;*
- *radiation transport calculations with special emphasis to radiation protection and experimental setups at the ELBE source as well as to the dosimetry in subcellular structures. Furthermore, these methods have been applied to the design of an industrial facility for product irradiations (polymer cross linking and sterilization of medical disposals).*

The department supplies the service of quality assurance of heavy ion tumour therapy by means of PET for the German Heavy Ion Therapy Project. In 2001 during 3 therapy beam times 39 patients have been treated, 35 of them with head and neck tumours, and, as a new development, 4 patients suffering from chordoma in the pelvic region. 23 patients were exclusively treated with ^{12}C ion beams, whereas to 16 patients a combined photon/carbon treatment was applied. Considering the irradiations within the pelvic region it is interesting to note that, despite of the high γ-ray attenuation, PET images of good quality could be taken with sufficient significance for reliable particle range and field position determination. For a total number of 1419 treatment fractions PET data have been acquired. As a result of the recent improvements of the physical beam model, which has been mainly induced by PET observations, the particle range for head and neck irradiations is precisely predicted by the treatment planning. Therefore, the PET data evaluation is increasingly focused onto the quantification of local deviations between planned and applied dose. Such deviations are caused by slight patient mispositioning or, even more important, by local changes of the tissue density distribution. The tomographic reconstruction was considerably improved by integrating a scatter correction into the iterative algorithm. Further research activities on PET are aimed at the development of an improved in-beam positron camera for the large clinical charged hadron therapy facility at Heidelberg, whose construction will be started in the year 2002. They comprise:

- *the design of a large solid angle positron camera in combination with a rotating ion beam delivery (gantry);*
- *the evaluation of new concepts of position sensitive γ-ray detectors with regard to their suitability for being operated in-beam;*
- *a feasibility study of proton therapy monitoring by means of PET;*
- *investigating the time microstructure of the γ-radiation as a condition for the layout of an efficient data acquisition system;*
- *the measurement of tissue dependent activity washout in order to improve the reliability of predicting β^+-activity distributions from the treatment plans.*

Collaborations

Heavy Ion Tumour Therapy

- *GSI Darmstadt*
- *Radiologische Klinik der Universität Heidelberg*
- *Deutsches Krebsforschungszentrum Heidelberg*
- *Institute for Bioinorganic and Radiopharmaceutical Chemistry (FZ Rossendorf)*
- *Soltan Institute for Nuclear Studies, Otwock-Swierk, Poland*

Cell Radiobiology at ELBE

- *Klinik für Strahlentherapie und Radioonkologie, TU Dresden*
- *Institut für Strahlenschutzphysik, TU Dresden*
- *Institut für Zoologie, TU Dresden*
- *Institute for Bioinorganic and Radiopharmaceutical Chemistry (FZ Rossendorf)*

Establishment of a Cell Culture Laboratory at ELBE

A. Panteleeva, J. Pawelke, E. Lessmann

Measurement of RBE values of photons in the energy range 10 - 100 keV are planned to be performed using the quasi-monochromatic channeling radiation source at the ELBE accelerator [1]. In order to study radiation effects on living cells, minimizing of side effects coming from the time consuming preparation procedures and transportation of the cell cultures is necessary. Therefore, a cell culture laboratory was established in the ELBE building to allow the straight preparation of the samples for irradiation and as fast as possible processing after it. Equipment for cell culture growth (two CO_2 incubators), for handling in sterile environment (a laminar flow box) and a cooled centrifuge are provided. The cell growth as well as the radiation induced effects can be observed with the help of an ordinary light microscope as well as of an inverse fluorescent microscope. The sterilisation of instruments and media is performed by hot air or hot steam and pressure sterilisation. There is equipment for water deionisation as well as chemical neutralisation of the disposed liquids. In the future, possibilities for the determination of radiation damage using radioactively labelled cells as well as growth of cells in different gas environment (N_2, O_2) are allowed in the laboratory. Furthermore, the laboratory is prepared for later use of genetically modified samples (genetic class S2).

The cell culture work started in May 2001. As biological endpoints for the first experiments at the ELBE photon source, clonogenic survival and micronuclei formation assays are chosen [2]. Preparation of the future experiments includes establishment of conditions for cell growth for different cell lines, optimisation of both assays in use and tests of cell carrier materials, which can be used in practicable irradiation unit. The cell lines under research in our laboratory up to now are NIH/3T3 (mouse fibroblasts, ATCC) and HH4dd (human skin fibroblasts, provided by Prof. Rodemann, Tübingen University).

In order to measure the RBE of X-rays at the horizontal ELBE beam, some requirements to the irradiation setup have to be fulfilled: (i) in order to minimise the attenuation of X-rays, the thickness of the cell substrate has to be in the order of $\leq$ 100 μm; (ii) the cell vessel has to be closed and to contain sufficient amount of medium (Fig. 1). The material of the substrate has to provide good attachment and cell proliferation. The growing conditions of the two cell lines were optimized for different substrate materials, and the properties of the most suitable are shown in Table 1. Capability of the cells to form colonies (plating efficiency), the control level of micronuclei formation and the cell proliferation by means of dye-exclusion assay were compared after the cells were growing on the studied substrates and standard material (polystyrene culture dish). The results are presented in Table 2, showing that the parameters of growth and proliferation are not changed by the studied substrate materials. However, the commercially available tissue culture insert PetriPerm, based on the Biofolie membrane (Sartorius, Göttingen) was chosen (thickness 25 μm), mainly because the transparent membrane allows observation of growth and performing of the micronucleus test directly on the membrane.

The future cell culture work at ELBE cell lab includes introducing of more cell lines (e.g. AG-01522 human fibroblasts, human mammary epithelial cells).

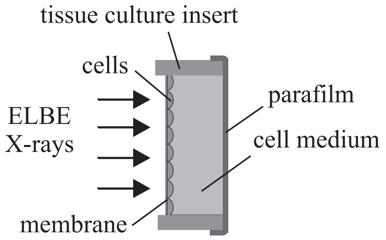

Fig. 1 *Design of the irradiation setup.*

Tab. 1 *Main membrane properties.*

Membrane material	additional treatment	growth of cells as a monolayer	transparent
Isopore [a] (polycarbonate)	poly-L-lysine	good	not
Biofolie [b] (Teflon)	not required	good	yes

Producers: [a]Millipore, Eschborn [b]Sartorius, Göttingen

Tab. 2 *Control levels of cell proliferation parameters - comparison of conventional cell culture vessels and membrane materials for the two cell lines.*

Cell line	3T3			HH4dd	
cell substrate	Plating efficiency [%]	BNC+MN [a] [%]	MN/ BNC+MN [b]	BNC+MN [a] [%]	MN/ BNC+MN [b]
Biofolie	35.9±1.7	2.2±0.2	1.10±0.06	3.4±0.4	1.09±0.04
Isopore	36.2±1.4	not possible, membrane not transparent			
polystyrene (culture flask)	33.0±1.6	1.7±0.3	1.02±0.02	3.3±0.5	1.04±0.03

[a] Fraction of binucleated cells with micronuclei [b] Number of micronuclei per binucleated cell with micronuclei

[1] W. Neubert et al., FZ Rossendorf, Wiss.-Tech. Ber. FZR-319 (2001) 41
[2] A. Panteleeva et al., This Report, p. 90

Determination of RBE of 25 kV X-Rays for Cell Survival and Chromosomal Damage

A. Panteleeva, K. Brankovic[1], W. Dörr[1], C. Hoinkis[1], J. Pawelke, D. Slonina[2], K. Spekl[1]

The determination of RBE of X-rays in the energy range 10 - 100 keV is important because of their wide application in radiology (e. g. mammography) and radiotherapy. Lately it was shown that the RBE value of X-rays from a 29 kV X-ray tube for neoplastic transformation of the human hybrid cell line CGL1 (HeLa/skin fibroblasts) is 3.4, whereas for survival it was 1.1 - 2.0 (reference radiation 200 kV X-ray tube) [1].

At the Medical Department of Dresden University the RBE value of X-rays from a 25 kV X-ray tube was determined for cell survival [2] and chromosomal damage (formation of micronuclei). The irradiation was performed with a tungsten anode therapy unit Darpaq 150-MC (operated at 25 kV, 20 mA, dose rate 1.7 Gy/min) and a conventional tungsten anode X-ray tube Isovolt 320/13 (operated at 200 kV, 20 mA, dose rate 1.2 Gy/min). The cell lines in use were: mouse fibroblasts NIH/3T3 (ATCC, USA), hamster fibroblasts V79 (ATCC, USA), primary neonatal human keratinocytes HEKn (TEBU, Germany), primary human skin fibroblasts HFIB (Biochrom, Germany).

The HFIB fibroblasts were not used in the survival assay because of lacking colony formation. A strong cell line dependence of the survival was found in the experiments. Applying the linear-quadratic model fit to the survival curves, the α and β values displayed in Table 1 were obtained. The 3T3 fibroblasts showed a strong decrease in survival after irradiation with 25 kV X-rays compared to the irradiation with 200 kV at high doses, which was not observed for the other cell lines. The RBE was calculated at 10 % survival and it was found to be not significantly different from 1 for all cell lines.

The second endpoint investigated was the induction of micronuclei which is a manifestation of cytogenetic damage. After irradiation, the cells are incubated in culture medium with cell line dependent concentration of cytochalasin B, which blocks the cytokinesis without blocking the karyokinesis. This allows to select the cells which have passed exactly one division after irradiation (binucleated cells). The micronuclei are chromosome fragments (or even whole chromosomes) closed by a nuclear membrane, which are formed during the cell division due to DNA damage. The severity of damage is determined by the number of binucleated cells with micronuclei; the number of micronuclei per binucleated cells with micronuclei is an indication of the quality of the damage. The V79 fibroblasts were not used in this assay, because of a lacking responsiveness to cytochalasin B. The fraction of binucleated cells was found to decrease with the increase of the dose, which shows the diminished division capability after irradiation. This effect is equally expressed for both radiation qualities. The frequency of binucleated cells with micronuclei, as well as the number of micronuclei per binucleated cell were found to be linearly dependent on the dose up to $\sim 5\,$Gy for all cell lines. Significantly higher induction of micronuclei was observed after irradiation with 25 kV X-rays in comparison to 200 kV X-rays (Fig. 1). The RBE-values for the different cell lines were found to be between 1.1 and 1.3.

Further experiments with monochromatic sources will allow detailed study of the X-ray energy dependence of the RBE. Such experiments are in preparation at the photon source at ELBE.

Tab. 1 *Parameters of the cell survival of fibroblasts (3T3, V79) and keratinocytes (HEKn) after irradiation with 25 kV and 200 kV X-rays.*

cell line	radiation quality	$\alpha(\pm$SEM) $[Gy^{-1}]$	$\beta(\pm$SEM) $[Gy^{-2}]$
3T3	25 kV	0.10 ± 0.05	0.070 ± 0.010
	200 kV	0.24 ± 0.02	0.022 ± 0.002
V79	25 kV	0.11 ± 0.04	0.035 ± 0.014
	200 kV	0.08 ± 0.02	0.032 ± 0.005
HEKn	25 kV	0.40 ± 0.10	0.048 ± 0.054
	200 kV	0.31 ± 0.03	0.048 ± 0.011

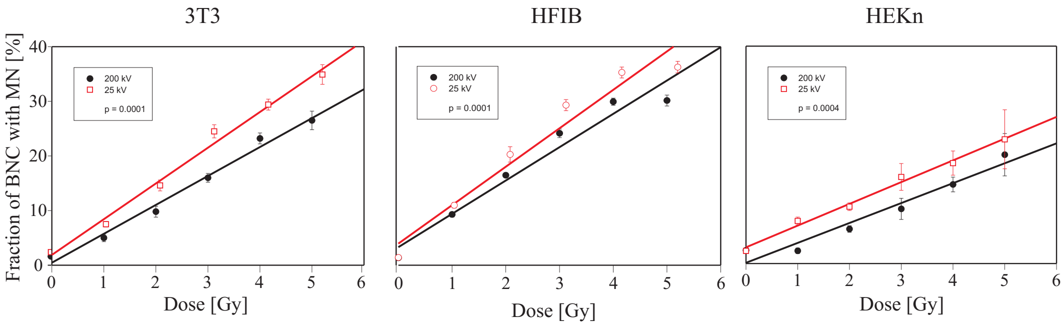

Fig. 1 *Dose dependence of the fraction of binucleated cells with micronuclei after irradiation with 25 kV (grey lines, open symbols) and 200 kV X-rays (black lines, closed symbols).*

[1] D. Frankenberg et.al., Stahlenbiologie und Strahlenschutz, Band I, TÜV-Verlag, Köln (ISBN 3-8249-0618-X) (2000) 27
[2] K. Brankovic et.al., Exp. Strahlenther. Klin. Strahlenbiol. 10 (2001) 71

[1] *Dept. Radiotherapy, Medical Faculty, TU Dresden*
[2] *Radiobiology Laboratory, Centre of Oncology, Krakow, Poland*

Design of an X-Ray Monochromator for the Channeling Source at ELBE

J. Pawelke, B. Beckhoff[1], B. Kanngiesser[2], M. Palm[3], A. Panteleeva, B. Stoevesandt[3]

One topic of research at the ELBE facility is the realisation of an X-ray source for radiobiological investigations. In a first project, quasi-monochromatic X-rays will be produced by electron channeling in diamond crystals which will be applied to determine the energy dependent relative biological effectiveness of photons in the range of $10 - 100$ keV. The channeling radiation (CR) source has been optimised in order to reduce the bremsstrahlung background to the unavoidable contribution from the diamond crystal. In a given energy interval, the intensity of the quasi-monochromatic CR dominates over the polychromatic bremsstrahlung background by more than one order of magnitude. However, the integral dose of bremsstrahlung is comparable to the CR dose [1].

Therefore, a first X-ray monochromator has been designed for CR of 19.4 keV maximum energy, assuming a cut of the channeling cone of 10 % FWHM energy spread to be used. This X-ray energy chosen is of relevance for mammography. It will be obtained by channeling of electrons of 15.5 MeV at the (110) plane (1→0 transition). Bragg reflection at the (002) plane of highly oriented pyrolytic graphite (HOPG) crystals was selected to achieve highest intensity of monochromatic radiation [2]. The determination of crystal curvature requires consideration of the Bragg reflection condition, the angular dependent intensity and energy distribution of the CR (calculated following the formalism given in [3]) as well as the practical limitations at the ELBE beamline such as CR source to monochromator distance of 1 m and focusing the reflected beam to a cell target of ≈ 3 cm^2 size at a distance of 2 m from the source (Fig. 1). Furthermore, aspects of the experimental HOPG design and the interaction of the X-rays with the crystals by use of a ray tracing code based on Monte Carlo methods [2] were also considered.

An optimal design was found to be a monochromator consisting of 15 steps (Fig. 2). The toroidal basic shape (cf. Fig. 1, rotation about a line which is parallel to x-axis passing Z_0) results in optimal focusing whereas the logarithmic shape of each step (approximated by a sector with radius R_M, cf. Fig. 1 left) fulfills optimal reflection condition. For this geometry with 0.5 mm thick HOPG crystals of 0.8° mosaicity, a transmission from CR source to cell target of 21.2 % is calculated. Neither moving the source a few mm along x- or z-axis nor changing the crystal mosaic spread within $0.6 - 1.0°$ will strongly change the reflected radiation. However, moving the source by 2 mm along y-axis reduces the total transmission to 18.6 %. The intensity of the reflected photons varies at cell target by ≈ 50 % which has to be further considered in cell irradiation procedure.

Currently, the best material and best production technology for manufacturing the monochromator mould which will be coated with the HOPG crystals is under investigation. Here, radiation hardness of the mould in combination with high precision of the final curvature is necessary.

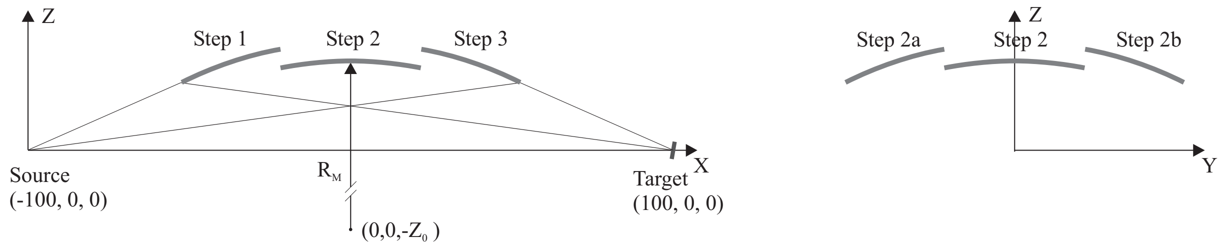

Fig. 1 *Schematic outline of the input geometry for monochromator design in meridional (left) and sagittal (right) direction.*

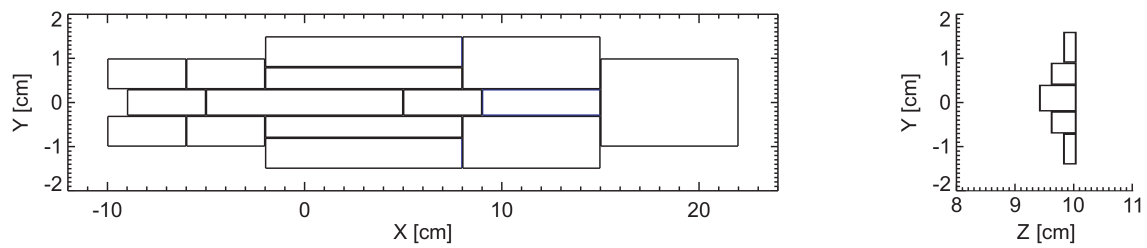

Fig. 2 *Geometry of the stepped monochromator design. Each step has a corresponding value of R_M and Z_0. The range of R_M and Z_0 is 955.3 – 1051.0 cm and 945.2 – 1041.4 cm, respectively, whereby $R_M > Z_0$.*

[1] W. Neubert et al., Proc. of the Int. Conf. Monte Carlo 2000, Lisbon, Portugal, Springer Berlin Heidelberg (2001) 123
[2] B. Beckhoff, PhD thesis, University of Bremen, signature DS-1732 (1995)
[3] A. Panteleeva et al., FZ Rossendorf, Wiss.-Tech. Ber. FZR-271 (1999) 95

[1] *Physikalisch-Technische Bundesanstalt, Berlin*
[2] *Technische Universiät Berlin*
[3] *Universität Bremen*

Considerations on Dosimetry for Measuring the RBE of Soft X-Rays at ELBE

J. Pawelke, A. Panteleeva, C. Hoinkis[1]

For determining relative biological effectiveness (RBE) of soft X-rays a quasi-monochromatic channeling source ($E_\gamma \approx 10-100$ keV) is being developed [1]. In preparation of RBE measurements at ELBE, experiments were performed with a conventional X-ray tube at TU Dresden. Several cell lines were irradiated with photons from a 25 kV soft X-ray tube and a 200 kV reference X-ray tube. Although the RBE values obtained show the enhanced damage from soft X-rays [2], there is a demand to determine it more precisely. Besides the irradiation with monochromatic soft X-rays, accurate determination of absolute dose delivered to the cell target is a crucial point for this.

Standard dosimetric technique is obtaining direct values for absorbed dose by air filled ionisation chambers (IC) which are optimised with respect to dose and energy dependence of response. A small soft X-ray chamber (23342) and a tube chamber (31003, PTW Freiburg) were used to measure the dose rate at target position before cell irradiation for the 25 kV and 200 kV X-ray tube, respectively. The dose delivered to cell is controlled by exposure time. However, ICs are integrating over photon energy and sensitive chamber volume.

Therefore, the dose was also calculated after determination of spectral photon flux density by considering the energy dependent energy absorption coefficient for water and integrating over energy range. For the measurement of the flux density of the 25 kV X-rays (Fig. 1), the necessary flux reduction was achieved by 25 μm slit tungsten collimator. Due to pratical limitations in reducing the flux density by using collimator or increasing the distance from the vertically emitting tube, a 200 kV X-ray model spectrum was calculated (Fig. 2). The comparison of the 25 kV and the 200 kV X-ray tube revealed that in the first case the main contribution to the dose (76 %) is coming from photons of energy $10-20$ keV and a minor one (20 %) by energies ≤ 10 keV, whereas in the second case, only 4 % of the dose is contributed by photons of $10-20$ keV but 61 % by photons of $20-60$ keV. Although useful in understanding the RBE energy dependence, the dose calculated in this way is less accurate than that one measured by IC. Here, the high dynamic range of ELBE beam intensity will allow more precise flux measurements without the use of any collimator. Furthermore, dose control by monitoring the ELBE electron beam intensity will be studied.

A suitable way to sample the depth dose distribution in a cell monolayer ($\approx 5\,\mu$m thick) seems to be the use of TSEE detectors, because they have a sensitive layer of the order of ~ 10 nm and show stable response [3]. If the detectors are irradiated in water or propanol (Table 1), the detector reponse remains stable and is only reduced due to attenuation in the liquid layer. In the presence of cell culture medium with its ingredients such as sugar, salts and proteins an unstable response with shift and change of the shape of the glow curve is observed. Therefore, TSEE detectors allow to sample the dose delivered to the cell approximating real conditions.

Tab. 1 *TSEE response of detectors covered with propanol or air after irradiation with low energy X-rays from ^{55}Fe source and high energy photons from ^{22}Na source.*

Detector type	Sensitive area [mm^2]	Spacing ^{a} [mm]	Response ratio air to propanol ^{b}	
			^{22}Na	^{55}Fe
I	43.0	1.0±0.1	1.0±0.1	28±2
II	146.4	1.0±0.1	1.0±0.1	68±6
III	146.4	2.4±0.2	1.4±0.3	112±4

^{a}) Detector to source distance, filled up with air or liquid
^{b}) Average of 5 repeated measurements

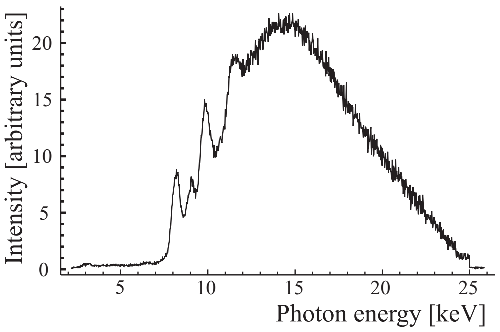

Fig. 1 *Energy distribution of the soft X-ray tube intensity (25 kV, tungsten anode, 0.3 mm Al filter), measured with a low-energy detector (XR100-CR, AmpTek, USA), corrected for the detection efficiency in the region $10-25$ keV.*

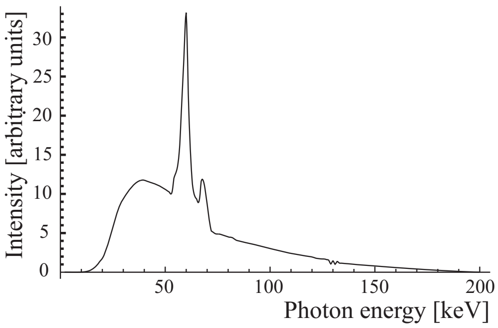

Fig. 2 *Energy distribution of the reference X-ray tube intensity (200 kV, tungsten anode, 0.5 mm Cu filter), calculated following the formalism given in [4].*

[1] W. Neubert et al., FZ Rossendorf, Wiss.-Tech. Ber. FZR-319 (2001) 41
[2] A. Panteleeva et al., This Report, p. 90
[3] J. Pawelke and A. Panteleeva, FZ Rossendorf, Wiss.-Tech. Ber. FZR-319 (2001) 102
[4] J.M. Boone and J.A. Seibert, Med. Phys. 24 (1997) 1661

[1] *Dept. Radiotherapy, Medical Faculty, TU Dresden*

Influence of Auger Electrons on Dose Distributions Simulated by PENELOPE

W. Neubert, W. Enghardt

It is well recognised that Auger emitters exhibit high-LET type radiotoxicity. The simulation of such processes requires reliable tools for radiation transport at very low energies. The updated code package PENELOPE [1] is capable of describing the transport of electrons and photons in arbitrary media down to energies as low as 100 eV and $\simeq 1$ keV, respectively. PENELOPE considers the relaxation process of an atom, excited by photon or electron impact, in which characteristic X-rays, photo- and Auger electrons are taken into account.

Table 1 *Auger electron radiation spectrum of ^{55}Fe [2]. The first column gives the Auger process, where the first letter denotes the shell with the vacancy before the Auger transition, the second and third letters indicate where the new vacancies are created, where X or Y denote shells above the specified ones. The last column gives the range in water.*

Transition	Energy/keV	Yield/decay	Range /μm
KLL	5.13	0.487	0.874
KLX	5.77	0.120	1.06
KXY	6.42	0.0082	1.27
LMM	0.56	1.41	0.0291
LMX	0.61	$\simeq$0.02	0.0341
MXY	0.049	0.23	0.00325

Iron was chosen since the code exactly treats the inner atomic electron shells up to the M subshells. Characteristics of Auger electrons emitted from ^{55}Fe [2] are given in table 1. The advantage of Fe is that by photon impact more than 60% of the photons are converted into K-shell Auger electrons [3] and about 90% of the electrons given in table 1 are tracked by PENELOPE. This way, the response of most of the components of the Auger electron spectrum can be studied separately. If the energy (e.g. for MXY Auger electrons) is below the above thresholds the dose will be deposited locally thus preventing a distinction of different transitions. In the next step we studied the track length distributions of selected Auger electron energies (see fig. 1). These data reproduce the ranges given in table 1. This reproduction is a necessary condition to apply PENELOPE for microdosimetric applications since related quantities are sensitive to the small-scale spatial distribution of the energy deposits along a track. The corresponding distributions (lower part of Fig. 1) show a regular behavior as low as 0.1 nm. Dose calculations were performed for a 2 μm thick layer of water. 15 keV photons impinging on a 0.1 μm Fe layer in front of this phantom generate flourescent X-rays, photoelectrons (7.87 and 8.62 keV) and Auger electrons the latter one's are stopped within the phantom thickness. The depth dose distribution in Fig. 2 shows a pronounced enhancement at low distances from the entrance. This effect cannot be asigned to characteristic flourescense radiation and photoelectrons which show another dose profile.

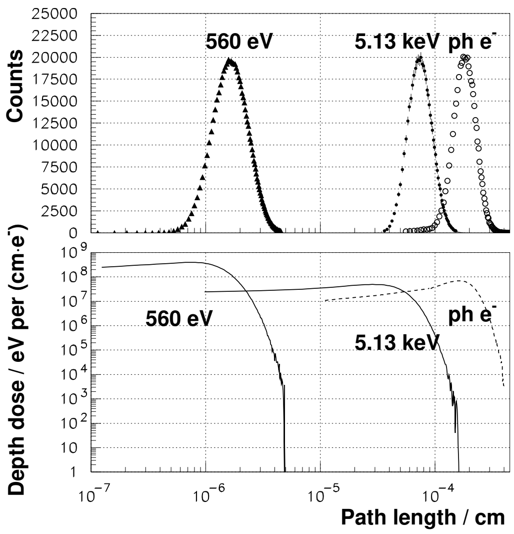

Fig. 1 *Upper part: Normalized track length distributions of low energy electrons corresponding to LMM and KLL Auger transitions, ph e$^-$ denotes photoelectrons from 15 keV photon impact on Fe as calculated by PENELOPE. Lower part: corresponding depth dose distributions.*

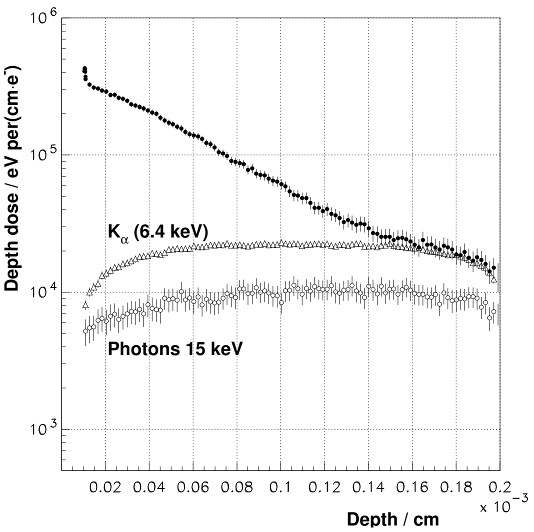

Fig. 2 *Depth dose distributions in water. Dots: 15 keV photons impinging on a 0.1 μm Fe foil in front of the specimen. Triangles: 6.4 keV Fe-K_α in water. Open circles: response of 15 keV photons in water.*

[1] F. Salvat et al., PENELOPE, A code System for Monte Carlo Simulations of Electron and Photon Transport, Proc. Workshop/Training Course OECD/NEA, 5-7 Nov.2001, NEA/NSC/DOC (2001) 19, ISBN: 92-64-18475-9
[2] R.W. Howell, Med. Phys. 19 (1992) 1371
[3] J. Stepanek, Med. Phys. 27 (2000) 1544

Electromagnetic Interactions Simulated by PENELOPE, FLUKA and GEANT4

H. Müller, B. Naumann[1], W. Neubert

The construction of setups at the experimental areas of the superconducting electron accelerator ELBE with respect to requirements of radiation protection are based on comprehensive calculations. In order to find optional solutions one has to be sure that the used codes reproduce experimental data related to the basic electromagnetic interactions within the necessary accuracy, especially at low energies. The incident energy of $20\,MeV$ which is typical for ELBE was chosen for an intercomparison of three code packages available in the public domain.

The code system PENELOPE [1] performs Monte-Carlo simulations of coupled electron-photon transport in arbitrary materials from $100\,eV$ for electrons and $1\,keV$ for photons to about $1\,GeV$. Electron and positron histories are generated on the basis of a mixed procedure which combines detailed simulation of hard events with condensed simulation of soft interactions.

The code FLUKA [2] originally written as hadron event generator handles now electromagnetic processes too. Differences concerning stopping power and bremsstrahlung production in electron and positron interactions are considered. The angular distribution of bremsstrahlung photons correlated with the energy are taken into account. FLUKA simulates the transport of all these radiation components and their reciprocal interactions at the same time. The lower thresholds for particle and photon propagation are $1\,keV$ limited by an upper energy of about $1000\,TeV$.

GEANT4 [3] is a toolkit for the simulation of the passage of particles through matter. Its application areas include high energy physics and nuclear experiments, medical, accelerator and space physics studies. Due to its object oriented design different processes and models can be easily implemented. The user decides which processes are relevant for his problem and which models to be used. In the present paper the standard package for energies down to $10\,keV$ and the low energy package for energies down to $250\,eV$ have been employed. The use of evaluated data files allows the application up to the GeV region.

In order to compare the results of the available codes a simple test arrangement was used. A disk of iron ($1\,cm$ in diameter and $1\,mm$ thick) was chosen as target arranged perpendicularly to the point-like incident beam of $20\,MeV$ electrons and photons. In the following we compare the energy spectra of electrons and photons emitted at the downstream side of the disk as calculated with the available codes.

The results for photon induced processes are shown in Fig. 1, that for electron induced ones in Fig. 2. There is a good agreement in case of incident photons. Only at the highest energies of the secondary electrons GEANT4 yields a bump, which is not observed in the PENELOPE and FLUKA results. For incident electrons a remarkable agreement was obtained (i.e. within the line widths) between the curves from PENELOPE, FLUKA and the standard version of GEANT4, while the results from the low energy package show distinct deviations up to a factor of about 4 in the high-energy part of the bremsstrahlung photons and about 50 % for the scattered electrons at energies around $5\,MeV$.

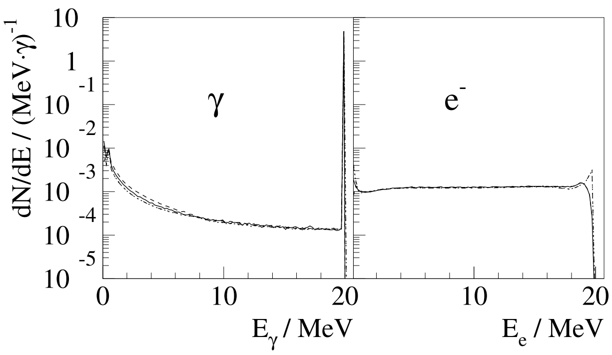

Fig. 1 *$20\,MeV$ incident photons: distributions of scattered photons and secondary electrons calculated with PENELOPE (full lines), FLUKA (dashed lines) and GEANT4 (dotted lines for standard, dashed-dotted lines for low energy package). The spike at $20\,MeV$ in the left panel belongs to transmitted photons.*

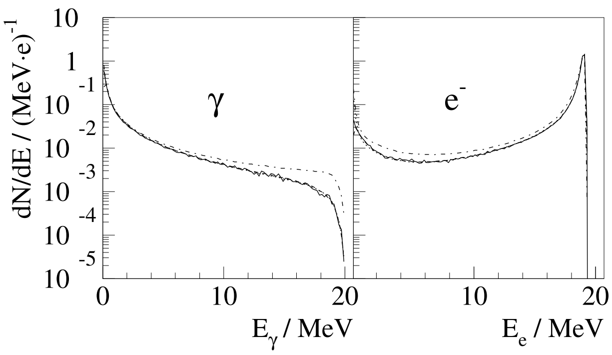

Fig. 2 *$20\,MeV$ incident electrons: distributions of bremsstrahlung and scattered electrons calculated with PENELOPE (full lines), FLUKA (dashed lines) and GEANT4 (dotted lines for standard, dashed-dotted lines for low energy package). Fluctuations in the PENELOPE distributions are due to lower statistics.*

[1] F. Salvat et al., PENELOPE, A code System for Monte Carlo Simulations of Electron and Photon Transport, Proc. Workshop/Training Course OECD/NEA, 5-7 Nov.2001, NEA/NSC/DOC (2001) 19, ISBN: 92-64-18475-9

[2] A. Fasso, A. Ferrari and P.R. Sala, Proc. of the Monte Carlo 2000 Conference, Lisbon, 23-26 Oct., 2000

[3] The GEANT4 Collaboration, http://wwwinfo.cern.ch/asd/geant4/geant4.html, Version 4.0

[1] *Institute of Nuclear and Particle Physics, TU Dresden*

Neutron Production by Photons and Electrons Simulated by FLUKA, MCNP4C2 and GEANT4-4.0

C. Beckert[1], H. Müller, B. Naumann[2], K. Noack[1]

Neutron production at the electron beam of ELBE proceeds as a two-step process via Bremsstrahlung with subsequent photo-neutron production. Envisaged research with neutrons concerns the interaction of neutrons with materials used for fission or fusion reactors [1]. Neutrons might also turn out to be a rather disturbing background for planned radio-biological studies [2]. Therefore, efforts are necessary to understand neutron production at ELBE.

In FLUKA the cross sections of photo-nuclear interactions in the region of the Giant Dipole Resonance are taken from tables or from parameterizations. Since the nuclear de-excitation is similar to that of a compound nucleus, the energy dissipation is treated by the PEANUT preequilibrium-evaporation module [3] of FLUKA.

MCNP is a general purpose Monte Carlo transport code for neutrons up to 20 MeV and for photons and electrons between 1 keV and 100 MeV. Photo-nuclear physics is implemented on the basis of evaluated data both for the photo-nuclear cross sections as well as for the distributions of the secondary particles [4].

GEANT4 takes parameterizations of available data for the calculation of the probability of photo-nuclear interactions. Final states are generated on the basis of the Chiral Invariant Phase Space model [5]. For the present considerations the standard package for electromagnetic interactions is used together with the low-energy package for neutron propagation, which is applicable from thermal energies up to about 20 MeV.

For a comparison of the above mentioned codes a test arrangement similar to that of the previous contribution [6] was used. The thickness of the iron disk is increased to 1 cm to get enough neutrons within reasonable computer times. Again, incident beams of 20 MeV photons and electrons interact with the target and the energy spectra of neutrons at the downstream side of the disk are calculated. The spectral distribution of photon induced neutrons is shown in Fig. 1, that of electron induced ones in Fig. 2. The results of the various codes show distinct differences. The most prominent discrepancy is the strong population of the ground state of the final nucleus of the (γ, n) reaction (the peak around 9 MeV) in case of the GEANT4-4.0 calculation, a feature not observed for the other codes. Experimental data are rather scarce, thus an independent verification is difficult. Also around 1 MeV the neutron yield differs between FLUKA and GEANT4-4.0 by nearly a factor of 4.

The neutron spectra from incident electrons (Fig. 2) reflect to a certain degree the properties of the (γ, n) reaction, because the electrons produce a broad distribution of Bremsstrahlung-photons (see Fig. 2 in [6]) which, in turn, are responsible for neutron production. The GEANT4-4.0 (γ, n) spectrum exhibits the largest intensity at high energies, and consequently also the neutrons from the two-step process, $e^- \rightarrow \gamma \rightarrow n$, extend to higher energies compared to the results from MCNP4C2 and FLUKA. In case of GEANT4-4.0 the statistical accuracy is insufficient for a reasonable comparison at lowest energies.

The details of the energy distribution of background neutrons produced in the beam tube are surely of minor importance for radio-biological studies. For the planned research with neutrons, however, the knowledge of energy distribution might be of decisive importance. Therefore, a similar comparison with ^{56}Fe replaced by Pb, the production target for neutrons, is of interest.

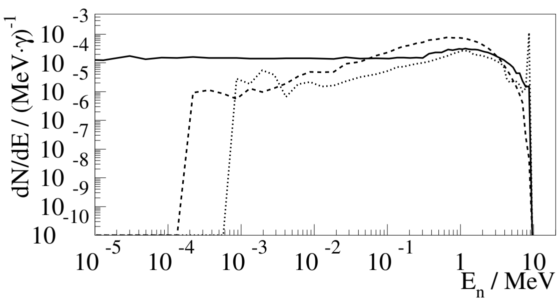

Fig. 1 20 MeV *incident photons: energy distributions of neutrons calculated with MCNP4C2 (full lines), FLUKA (dashed lines) and GEANT4-4.0 (dotted lines).*

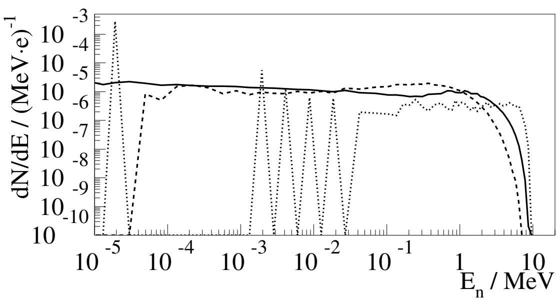

Fig. 2 *The same as Fig. 1 but for incident electrons.*

[1] H. Freiesleben et al., Annual report 1997, FZR-215 (1998) 14

[2] W. Neubert et al., Annual report 2000, FZR-319 (2001) 41

[3] A. Fasso et al., Proc. of the III Spec. Meeting on Shielding Aspects, Sendai (1997) 61

[4] M.C. White, Los Alamos National Laboratory report LA-13744-T (2000)

[5] P. V. Degtyarenkoet et al., Eur. Phys. J. A9 (2001) 421

[6] H. Müller et al., This Report, p. 94

[1] *FZR, Institute of Safety Research*

[2] *Institute of Nuclear and Particle Physics, TU Dresden*

X-Ray Imaging of Phase Transition and Flow Phenomena in Liquid Metals: A Feasibility Study

S. Eckert[1], W. Enghardt, W. Neubert, H. Neumann[1], J. Pawelke

The study is aimed at a first estimation of the experimental conditions for visualizing phase transition and flow phenomena in liquid metals by means of X-rays. As an example we consider the solidification of the molten alloy $Pb_{15}Sn_{85}$. Dendrites of pure lead having a thickness of about 50 μm and a length of about 200 μm are preticipated from the melt at the liquid-solid interface. In a first step the optimum X-ray energy for this imaging problem has been estimated by means of a signal-to-noise-ratio (SNR) analysis. The SNR is given in the worst case, where the X-rays on their path through the sample pass only one dendrite, by the equation

$$SNR = \frac{|\phi_A - \phi_D|}{\sqrt{\phi_A + \phi_D}} \tag{1}$$

where

$$\phi_A = \phi_0 \, e^{-\mu_A(E_X) d_A} \tag{2}$$

and

$$\phi_D = \phi_0 \, e^{-\mu_A(E_X)(d_A - d_D) - \mu_D(E_X) d_D} \tag{3}$$

describe the attenuation of the incident photon flux ϕ_0 by a molten sample of the thickness d_A without and with one dendrite (thickness $d_D = 50$ μm), respectively. The linear attenuation coefficients $\mu_A(E_X)$ and $\mu_D(E_X)$ of the $Pb_{15}Sn_{85}$ melt ($\varrho = 7.6$ g cm^{-3}) and of the Pb-dendrites ($\varrho = 11.2$ g cm^{-3}), respectively, in dependence on the photon energy E_X have been taken from [1]. From medical imaging it is known that useful images should have a minimum SNR of 4. Thus, we calculated the number of incident photons in dependence on their energy under these conditions for samples of 1 and 2 mm thickness d_A. The results depicted in Fig. 1 suggest an optimum photon energy for this imaging situation between 100 and 140 keV.

Since this simple SNR analysis does not take into account the image degradation due to the interaction of the X-rays with matter, a more detailed photon transport calculation by means of the GEANT simulation code has been performed. Five boxes ($50 \times 50 \times 200$ μm^3), equally spaced by 50 μm are supposed to be the solid lead dendrites. They were inserted into the melt of $Pb_{15}Sn_{85}$ confined to $475\,\mu$m$\times 2\,$mm$\times 200\,\mu$m. This phantom was irradiated with a parallel X-ray beam (0.5×0.1 mm^2) with energies from slightly above the K absorption edge of Pb (88 keV) to 140 keV to scan the energy range of the minimum in Fig. 1. The interaction of the photons and their secondary electrons with the samples is described by taking into account photoeffect, Compton and Rayleigh scattering, multiple electron scattering as well as collision and radiative stopping. A comparison of the contrast of the distributions of photons after penetrating the sample (Fig. 2) reveals that monochromatic X-rays of 100 keV should be the optimum radiation quality. If a conventional X-ray source (200 kV, 20 mA) is applied, images with a $SNR \geq 4$ require an irradiation time of about 0.5 s (assuming a focus-object-distance of 45 cm and a photon detector of 10 % efficiency). This imaging time is expected to be reduced by two orders of magnitude, when quasi-monochromatic channeling X-rays of 100 keV will become available by irradiating diamond crystals [2] with the ELBE electron beam of 40 MeV.

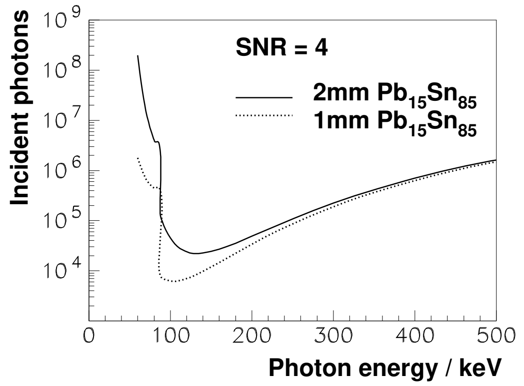

Fig. 1 *Number of incident photons per image pixel necessary to obtain an SNR of 4 as function of the photon energy.*

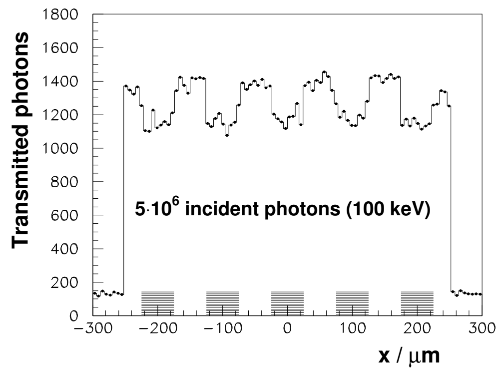

Fig. 2 *Simulated lateral distribution of photons after penetrating the sample model obtained for $5\cdot 10^6$ histories of 100 keV X-rays. The hatched zones indicate the location of Pb dendrites.*

[1] http://physics.nist.gov/PhysRefData/XrayMassCoef/tab3.html
[2] A. Panteleeva et al., FZ Rossendorf, Wiss.-Tech. Ber. FZR-271 (1999) 95

[1] *FZR, Institute of Safety Research*

Radiation Transport Calculations for an Industrial Low-Energy Electron Accelerator

W. Neubert, W. Enghardt, M.N. Andronenko[1], B. Naumann[2], K. Konschak[3], W. Schumann[3]

The use of electron accelerators in industry involves a broad and continuously growing range of applications [1, 2], e. g. crosslinking of polymers, sterilization of food and medical disposables as well as the treatment of environmental waste. For such applied purposes the efficiency of the irradiation process is of primary importance and this requires the layout of the beam delivery system of accelerators to be carefully optimized.
A further motivation for such calculations is given by radiation protection issues and the necessity to design reliable shieldings against the primary electrons and the secondary radiation of bremsstrahlung and neutrons. Thus, for a typical industrial accelerator delivering an electron fan beam of $10\,mA$ at $E_e < 10\,MeV$ we performed such calculations by means of the public domain radiation transport codes GEANT [3] and FLUKA [4].

In particular the following calculations were performed:

- The modelling of the fan beam and its broadening by scattering in air.
- The simulation of the spatial and spectral distributions of bremsstrahlung from a tungsten-copper radiator at an electron incident energy of $E_e = 9.8\,MeV$.
- The description of neutron production in the tungsten-copper radiator at $E_e = 9.8\,MeV$, due to the (γ,n) threshold of $8.1\,MeV$ for tungsten [5].
- The activation of the radiator materials W and Cu by the production of ^{181}W, ^{185}W, ^{187}W, ^{64}Cu and ^{66}Cu.
- The calculation of dose rate distributions in polyethylene pipes (for polymer crosslinking) delivered by electron beams of $E_e = 4.0\,MeV$ and $9.8\,MeV$ as well as by $9.8\,MeV$ bremsstrahlung in dependence on the pipe diameter and the beam incidence.
- The calculation of dose rate distributions in medical disposables (for sterilization) of different mass density delivered by $9.8\,MeV$ and $4.0\,MeV$ electrons and $9.8\,MeV$ bremsstrahlung.

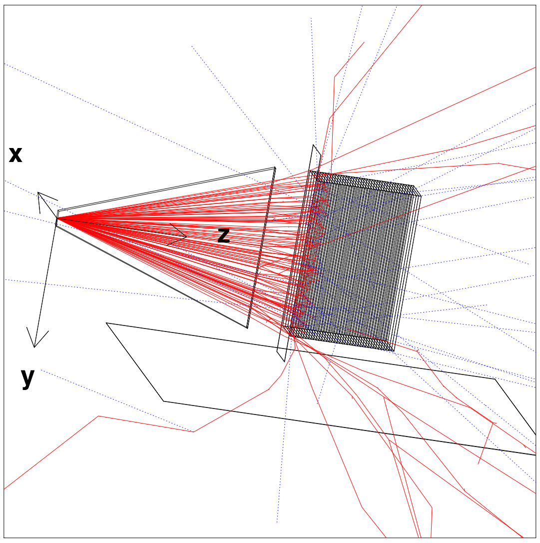

Fig. 1 *Perspective view of the irradiation setup with the fan electron beam extracted into air through a vacuum window. The gray box shows the products to be irradiated. Parralelograms are monitor areas.*

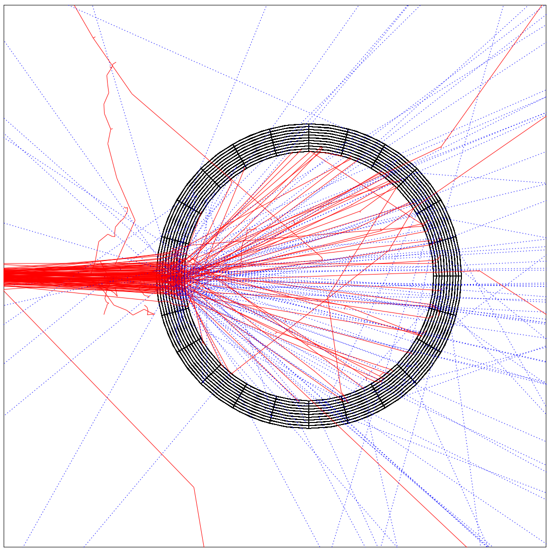

Fig. 2 *Presentation of electron tracks (dashed-dotted)incident on a pipe subdivided into sectors and ring zones. Photons produced by interaction with air and polyethylene are shown as thin dotted lines.*

[1] W. Mondelaers et al., Nucl. Instr. A 368 (1995) 278
[2] J. Mckeown et al., Radiation Physics and Chemistry 53 (1998) 55
[3] GEANT - Detector Description and Simulation Tool, CERN Program Library W 5013, 1994
[4] A. Fasso, A. Ferrari, J. Ranft and P. Sala, FLUKA-98 (http://AliSoft.cern.ch/offline/fluka/manual)
[5] B. Forkman and R. Peterson, Handbook on Nuclear Activation Data, IAEA, Techn. Rep. 273 (1987) 787

[1] *St.Petersburg Institute of Nuclear Physics, Gatchina, Russia*
[2] *Institute of Nuclear and Particle Physics, TU Dresden*
[3] *Gamma Service Produktbestrahlung GmbH, Leipzig, Betriebsteil Radeberg*

An Interactive Approach for Local Dose Quantification from In-Beam PET Data [B, G]

K. Parodi, W. Enghardt

The in-beam PET monitoring of carbon ion therapy supported the reliability of the treatment planning and patient positioning procedures at the GSI Darmstadt facility [1]. However, in some cases it detected deviations of the measured and the predicted β^+-activity distributions, due to minor inaccuracies in patient positioning or local changes of patient anatomy [1]. These discrepancies may correspond to small deviations of the applied and planned dose. Hence, a local dose quantification from PET images shortly after each therapeutic irradiation is highly desirable. Due to the lack of a feasible solution for the inverse problem relating the β^+-activity to the dose, an interactive approach has been considered. The implementation has been based on the dedicated tool used for the visualization of the PET measured and predicted distributions as contour plots superimposed onto X-ray CT images [2]. In case of deviations, an interactive modification of the patient CT consisting either in geometrical transformation (translation and rotation) or in local Hounsfield unit (HU) modifications in user-selected regions of interest (ROI) can be performed. The reliability of the modification is tested by a recalculation of the β^+-activity distribution with and without the CT changes. Actually, only the spatial distribution of β^+-decays is computed, in order to avoid blurring due to the imaging procedure. The calculation is local and analytical, in order to reach a "fast" (within few minutes) response. Only the pencil-like beams crossing the chosen ROI are taken into account. The depth-distribution of the main β^+-isotopes (^{11}C, ^{15}O and ^{10}C) is extrapolated from the PET database (DB) [3] containing the spatial distributions of positron emitters produced in PMMA ($C_5H_8O_2$) by ^{12}C beams of all the energy values used for therapy. The DB information is combined with the irradiation strategy (ion energy, fluence and position) and with the patient anatomy by means of the HU-ion range correlation [3], [4] and the stoichiometric calibration of the CT numbers suggested in [5]. The lateral-distribution is assumed to be Gaussian with a FWHM dependent on the beam focus and the average positron range in tissue. The lateral spread of the beam in depth is neglected. The distribution of β^+-decays is deduced from the isotope production and the time interval between the beam delivery and the end of the PET acquisition. If the recalculation supports the modification, a new dose distribution based on the elaborated CT is obtained by means of the treatment planning software [4]. Fig. 1 shows an example. For this patient an extreme but plausible tissue reduction was assumed on the basis of range and anatomical symmetry considerations. A new CT scan confirmed the conjecture. In such cases a new treatment plan may be defined, according to the physician's decision. Hence, the interactive approach can give an important feedback. The optional introduction of imaging effects on the recalculated distributions for a more direct comparison with the reconstructed PET images is under development. In particular, the effects of minor CT modifications on the PET attenuation corrections are currently studied. Moreover, the sensitivity and accuracy of the method as well as the potential of real quantitative PET data for local dose quantification are under investigation.

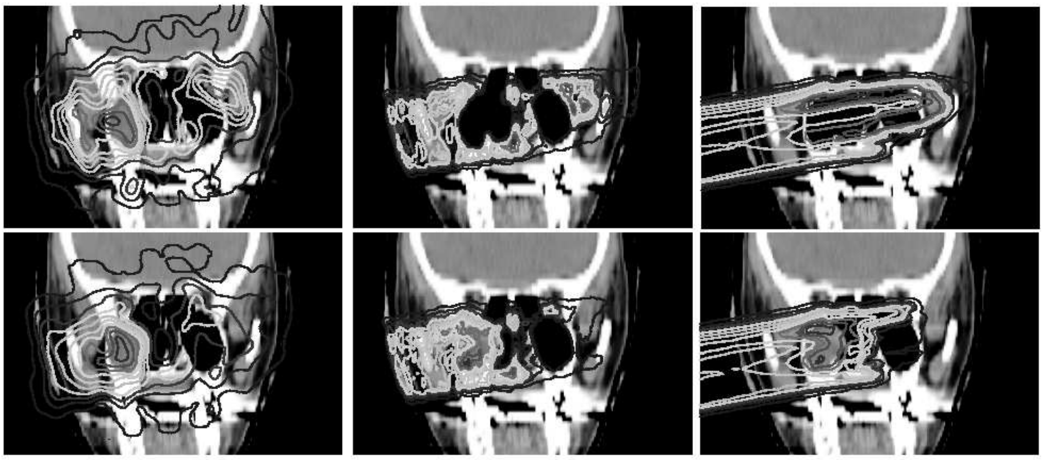

Fig. 1 *Left: Higher activation at the distal edge of the portal (entering the patient from the left of the picture) in the PET measurement (up) in comparison with the prediction (down). Middle: The recalculation with (up) and without (down) CT modification well resembles the PET images (left), thus supporting the hypothesis. Right: The effect on the recalculated dose distribution (up) in comparison with the planned one (down) is evident and in agreement with the PET observation.*

[1] W. Enghardt et al., FZ Rossendorf, Wiss.-Tech. Ber. FZR-271 (1999) 89
[2] F. Pönisch et al., FZ Rossendorf, Wiss.-Tech. Ber. FZR-271 (1999) 91
[3] B. G. Hasch, PhD Thesis, Dresden University of Technology (1996)
[4] M. Krämer et al., Phys. Med. Biol. 45 (2000) 3299
[5] W. Schneider et al., Phys. Med. Biol. 45 (2000) 459

A Scatter Correction for Iterative Tomographic Reconstruction[G]

F. Pönisch, W. Enghardt

A fully 3D reconstruction algorithm based on the Maximum Likelihood Expectation Maximization (MLE) algorithm has been developed for reconstruction of images from data taken by the limited angle double head camera BASTEI [1]. The process of photon scattering considerably influences the image quality in PET. For head and neck tumors about 30 % of the registered true coincidences are influenced by Compton or Rayleigh scattering, which may deteriorate the correspondence between the source and the reconstructed radioactivity distribution especially in such highly inhomogeneous regions of the human body like the head and neck. Therefore, a scatter correction is required.

The scatter correction algorithm needs the information on the tissue composition and density only within and nearby the camera field of view. This is derived from the X-ray computed tomograms (CT) of the patient (taken for treatment planning purpose) which are automatically combined with a CT of the head rest using characteristic landmarks [2]. This data set is the basis for the calculation of the attenuation correction factors. The measured lines of response (LOR) are corrected for the individual detector efficiency and the length of the emission line within the image space. The expectation step of the MLE-algorithm [3] is intended for modelling the imaging process in emission tomography. The classical algorithm of Shepp and Vardi [3] estimates the forward projection by computing the ray sums in each projection. We modified this procedure by applying the attenuation correction factors y_i^{att} to the forward projection and adding furthermore, the scattered components y_i^{scatt}:

$$x_j^{(n+1)} = x_j^{(n)} \cdot \sum_{i=1}^{I} \frac{a_{ij} \cdot y_i^*}{y_i^{att} \cdot \sum_{j'=1}^{J} a_{ij'} \cdot x_{j'}^{(n)} + y_i^{scatt}}. \quad (1)$$

$x_j^{(n)}$ denotes the activity distribution after the n-th iteration step, y_i^* is the modified measured projection for the i-th channel and a_{ij} is the element of the transition matrix.

To calculate the quantity y_i^{scatt} we follow the approximation of Watson [4], the Single Scatter Simulation (SSS). This algorithm simulates the scatter coincidences y_i' in a given LOR i by single Compton scattered events only. Therefore, the total number of scattered events N_{scatt} obtained from the SSS calculation has to be normalized to the number of acquired coincidences N_{meas}. We calculate the global scatter fraction (SF) by means of an additional Monte Carlo (MC) simulation from the n-th solution:

$$SF = \frac{N_{scatt}}{N_{total}}. \quad (2)$$

The simulation uses the activity distribution of the previous iteration step and the information of the attenuation map. The MC code has been optimized for accuracy and executing time. The number of histories has been chosen that the statistical error in the calculated SF is less than 0.3 %. Watson [4] has shown that a single scaling factor is sufficient for the total scatter distribution. By means of the SF one can estimate the number of scattered events from the measured one. From this follows the normalized scatter contribution of the coincidence channel:

$$y_i^{scatt} = y_i' \cdot \frac{SF \cdot N_{meas}}{\sum_i y_i'}. \quad (3)$$

Introducing (3) into (1) yields the modified forward projection for each iteration step.

The new reconstruction algorithm has been validated for experimental data. The scatter corrected β^+-activity distributions from phantom experiments as well as patient data show a good agreement with our expectation. The Figure 1 shows the profile of the reconstructed PET image with a size of $256 \times 128 \times 100$ voxels from a ^{22}Na point-like source, which was placed in a water filled cylindrical phantom (diameter 15 cm, height 15 cm). The removal of the scatter components after applying the scatter correction algorithm is obvious.

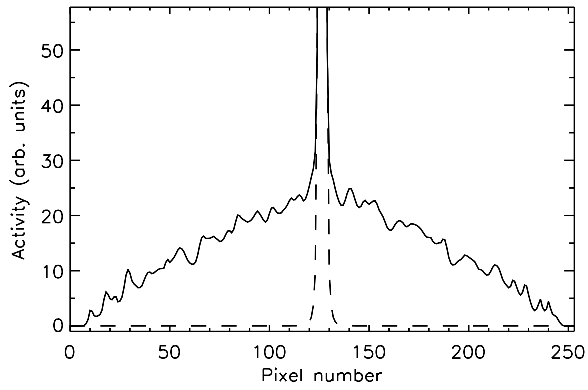

Fig. 1 *Profile of the reconstructed PET image of a point-like source in a water filled phantom. The solid curve is the reconstructed data set without scatter correction; the dashed curve is the data set using the scatter correction algorithm.*

[1] K. Lauckner, FZ Rossendorf, Wiss.-Tech. Ber. FZR-264 (1999) 70
[2] F. Pönisch et al., FZ Rossendorf, Wiss.-Tech. Ber. FZR-319 (2001) 95
[3] L.A. Shepp, Y. Vardi, IEEE Trans. Med. Imag. MI-1 (1982) 113
[4] C.C. Watson et al., in Three-Dimensional Image Reconstruction in Radiation and Nuclear Medicine (1996) 255

Benchmark Tests for an Iterative Tomographic Reconstruction Algorithm [G]

F. Pönisch, W. Enghardt, M. Schlett

PET images for therapy quality control, which are reconstructed from data that are acquired in-beam during heavy ion tumour irradiations at the therapy facility of GSI Darmstadt, have to be available as shortly as possible after finishing the treatment fraction, however, at the latest before applying the next daily dose fraction. The applied reconstruction technique - a true 3 dimensional Maximum Likelihood algorithm [1] - requires high computational power. Furthermore, a steady increase of the maximum number of patients treated per day and more sophisticated and thus time consuming reconstruction techniques as e.g. the scatter correction introduced recently [2], and new real-time data evaluation concepts [3] may lead to an overload of the Silicon Graphics® Inc. (SGI) Power Challenge™ workstation equipped with 6 R8000 processors, which has been exclusively dedicated to the computations connected with PET for therapy control [4]. Thus, we have investigated the possibility to replace this workstation in a cost effective way by personal computers since their computing power has rapidly increased during the last years. The performance of the SGI-system and Intel® compatible Linux® PC have been compared (further specifications see Tab. 1) running C-code implementations of the maximum likelihood tomographic reconstruction for PET data acquired during the irradiation of 2 patients (Tab. 2).

	CPU	Clock cycle / MHz	Cache size / kBytes
SGI	R8000	75	4096
PC-Intel	Pentium III	1000	256
PC-AMD	Athlon MP	1200	256
PC-Intel	Xeon	2000	256

Tab. 1 *Parameter of the computer platforms used for this benchmark test.*

For this test, irradiation portals, which require rather large PET image spaces of about 1.3 - 1.4 million voxels and therefore, a long reconstruction time have been chosen. Normally, the size of the image space is 1 million voxels. The other parameter that determines the reconstruction time is the number of registered valid coincidences during the PET scan. The mean value is about 80000 and, therefore, we have chosen PET scans with a number of valid events significantly below and above this mean. Finally the influence of different C-compilers on the run time has been studied.

Patient	Valid coincidences	Image space size (voxels)
1	40400	1260000 ($150 \times 100 \times 84$)
2	156800	1368800 ($118 \times 100 \times 116$)

Tab. 2 *Parameter of the reconstructions for 2 patients.*

The results of our benchmark test are shown in Table 3 and may summarized as follows:

(*i*) The running of the new scatter correction reconstruction algorithm [2] is not feasible on the SGI-system. The code has to be migrated to PCs with state of the art CPUs. The reconstruction algorithm with scatter correction runs faster on the most advanced machines than the original reconstruction (without scatter correction) on an R8000 (see bold figures in Table 3). From this it is estimated that 3 Intel® Xeon™ CPUs (2 GHz) will be sufficient to fulfil the current needs (10 - 15 patients per day) of computing power for the PET quality control of heavy ion therapy at the GSI Darmstadt facility.

(*ii*) The run time is strongly dependent on the applied C-compiler. Whereas the performance of the Xeon™ CPU is superior for the Intel-compiler, the Athlon™ CPU runs the reconstruction code processed by means of the GNU-compiler(gcc-2.95) in the most efficient way.

Patient	Host	CPU	Reconstruction Time / min: GNU-Compiler with sc***	Intel-Compiler with sc.	Intel-Compiler without sc.	Time ratio $\frac{\text{with sc.}}{\text{without sc.}}$
1	SGI	R8000	-	338*	**59***	5.7
	PC-Intel	Pentium III	96	76	24	3.2
	PC-AMD	Athlon MP	61	62	22	2.8
	PC-Intel	Xeon	65	**37****	10**	3.7
2	SGI	R8000	-	981*	**216***	4.5
	PC-Intel	Pentium III	220	191	96	2.0
	PC-AMD	Athlon MP	132	144	90	1.6
	PC-Intel	Xeon	137	**97****	36**	2.7

Tab. 3 *Comparison of the reconstruction time on different computers, reconstruction algorithm and compilers for 2 patients, * MIPS C Compiler on SGI system, **Intel Xeon optimized code, ***sc-scatter correction.*

[1] K. Lauckner, FZ Rossendorf, Wiss.-Tech. Ber. FZR-264 (1999) 70
[2] F. Pönisch, W. Enghardt, This Report, p. 99
[3] K. Parodi, W. Enghardt, This Report, p. 103
[4] R. Hinz, Diploma-Thesis, Chemnitz University of Technology (1995)

In-Beam PET Measurements of Proton-Induced β^+-Activity [B,G]

K. Parodi, W. Enghardt, T. Haberer[1]

The important impact of in-beam PET on the quality assurance of carbon ion therapy has been proven by the clinical experience at GSI Darmstadt [1]. The main achievements are *(i)* the monitoring of the maximum carbon ion range, *(ii)* the verification of the field position and *(iii)* the detection of unpredictable deviations of the real treatment from the planned one due to minor errors of the patient positioning or local changes of the patient anatomy (e.g. filling of cavities by mucus) [2]. Based on these results and motivated by the proposed dedicated proton and heavy ion (up to oxygen nuclei) therapy facility at Heidelberg [3], the potential extension of the PET technique to the monitoring of proton therapy is under investigation. In our first experiment [4] three mono-energetic proton beams (energy: 110, 140, 175 MeV; mean intensity: $7 \times 10^7 - 5 \times 10^8$ ions/s) were stopped in targets of PMMA ($C_5H_8O_2$) placed in the centre of the field of view of the in-beam positron camera installed at the GSI heavy ion therapy facility. Each PET measurement was taken over 10 min of irradiation and 20 min of decay. The amount of β^+-activity was found to be three times (3.2 ± 0.4) larger than that induced by carbon ions at the same range and applied physical dose. The lateral profile of the reconstructed activity distributions (Fig. 1) was found in good agreement with calculations [3] of proton beam broadening in depth. These two observations support the sensitivity of the PET method to detect field mispositioning or anatomical changes of the patient in the proton case, too. The control of the maximum proton range is a more challenging issue, since protons cannot suffer the projectile fragmentation process which leads to a peaked activity distribution in close proximity to the dose maximum in the carbon ion case. The reconstructed β^+-activity depth-profiles were well reproduced in shape by the production of the main positron emitters (^{11}C and ^{15}O) calculated on the basis of experimental cross-sections and the proton flux given by the FLUKA Monte Carlo code (Fig. 2). The shown reconstructed datasets contain events measured during the irradiation and later than 10 min after finishing the irradiation, in order to include and rule out the contribution of the short-lived ^{15}O, respectively. There is a unique relation between the position of the distal slope of the depth-activity curve (e.g. the 50% level), mainly determined by the energy thresholds of the fragmentation reactions, and the primary proton range. In our case the 50% level of the distal part of the measured and simulated profiles was found at about 6 mm lower penetration depth than the range. A very weak (< 0.5 mm) dependence on the initial energy and on the ^{15}O contribution was observed. The spatial activity-range correlation supports the possible extraction of range information by means of a comparison between measured and realistically calculated activity distributions, as done in the carbon ion case. The achievable accuracy is the crucial parameter, since millimeter precision is required. First simulation investigations of proton irradiation with a spread out Bragg peak [4] suggest that a millimeter control of the maximum proton range may be feasible. Future experiments at GSI Darmstadt are planned in order to measure the minimum proton range difference that can be resolved by the in-beam limited angle PET scanner. This will allow a final conclusion on the feasibility and achievable precision of proton range monitoring to be drawn. As a general remark we note that the in-beam technique is recommended in order to exploit the higher activity signal without losing the main contribution coming from ^{15}O in the case of patient irradiation and to acquire data directly in the treatment position.

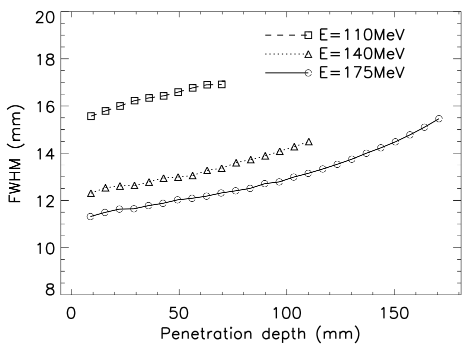

Fig. 1 *Lateral width of the β^+-activity profile versus depth in the central plane of the positron camera field of view for the three proton irradiations.*

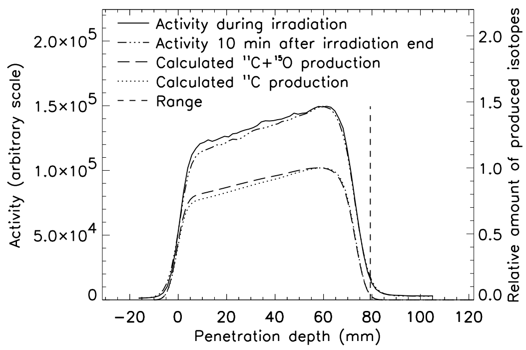

Fig. 2 *Reconstructed β^+-activity depth profiles in comparison with calculated isotope production for the 110 MeV proton irradiation (see text for explanation).*

[1] W. Enghardt et al., Nucl. Phys. A 654 (1999) 1047c

[2] W. Enghardt et al., FZ Rossendorf, Wiss.-Tech. Ber. FZR-271 (1999) 89

[3] K. D. Gross and M. Pavlovic (eds), Proposal for a dedicated ion beam facility for cancer therapy, Darmstadt (1998)

[4] K. Parodi, W. Enghardt and T. Haberer, Phys. Med. Biol. 47 (2002) 21

[1] *Gesellschaft für Schwerionenforschung Darmstadt*

The Evaluation of Carbon Ion Therapy PET Data within the Time Domain

C. Kausch[1], W. Enghardt

A large fraction of the positron emitters produced during the heavy ion therapy treatments are ^{11}C fragments with a half-life of 20.4 min. The activity accumulates during the irradiation in bony structures, whereas it is washed out in well vascularized tissue (e. g. the brain). This leads to discrepancies between the measured and the simulated PET images [1] and, therefore, a definitive statement on the accuracy of the dose deposition may be complicated or even impossible. Since the PET data are recorded in list mode, it is possible to evaluate the β^+-activity both in space and time [2]. To obtain tissue dependent washout data from the large amount of PET scans acquired for more than 100 patients treated at the GSI therapy facility, a software tool has been developed. In a first step volumes of interest - VOI - (i. e. tissue regions where the washout is to be determined) are interactively selected in images showing the β^+-activity distribution superimposed onto X-ray computed tomograms (CT) as shown in Fig. 1.

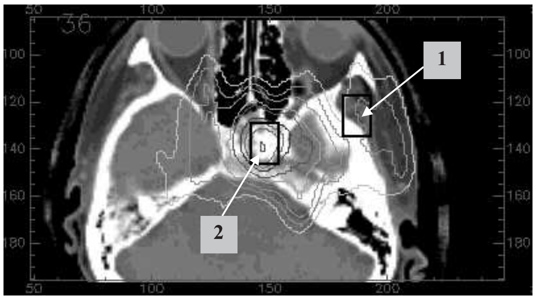

Fig. 1 *Transversal CT-image with the β^+-activity distribution through the head of a patient. The black boxes mark the examined VOIs with large (1) and low (2) washout.*

In the second step the time histogram of those lines of response, which intersect the VOI, is constructed and an effective lifetime can be calculated by means of a fitting procedure (Figs. 2 and 3). For precise fitting results the signal-to-noise ratio of the time histograms should be large. As the count rate is notoriously poor in PET studies performed simultaneously with the therapeutic irradiations and the available time intervals are short compared to the half-life of ^{11}C, it is planned for the future to sum up the PET-measurements for all therapy fractions of a certain patient and portal. Although this has not been implemented yet, the feasibility of the concept can be demonstrated for a treatment during which the beam delivery was interrupted by more than 15 min. Fig. 1 shows a transversal slice of the CT-images of the head, with the β^+-activity distribution superimposed. VOI (1) is located in a region with large blood flow whereas VOI (2) is placed in the skull base (bone). The corresponding time distributions are shown in Figs. 2 and 3, respectively. The relaxation of activity is an exponential process as well as the washout of emitter concentration. Thus, the measured time dependent count rate $c(t)$ is fitted to

$$c(t) = p_1\, e^{-\frac{t}{\tau_P}} + p_1\, e^{-\frac{t}{\tau_C}}\,, \qquad (1)$$

where p_1 is the normalization factor, τ_P and $\tau_C = 1766\,\mathrm{s}$ are the mean-lives for the activity washout and the ^{11}C decay, respectively. For comparison the decline of activity due to ^{11}C decay only is shown by the grey curve.

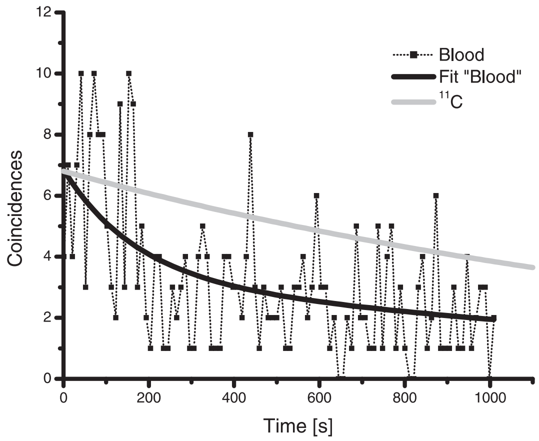

Fig. 2 *PET count rate versus time for VOI (1) with high perfusion. The black line shows the exponential fit of the data, the grey line shows decline due to ^{11}C decay only. The list mode data are rebinned into 10 s time intervals.*

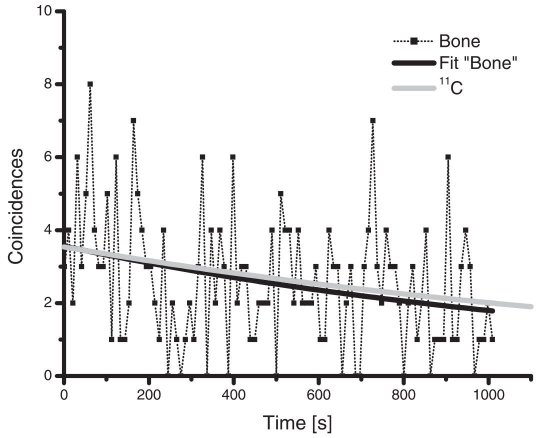

Fig. 3 *PET count rate versus time for VOI (2) with low perfusion.*

Whereas for the soft tissue in Fig. 2 an effective mean-life of $\tau_P = 165\,\mathrm{s}$ has been found, the emitter concentration in the bone, shown in Fig. 3, drops much slower ($\tau_P = 1220\,\mathrm{s}$).

[1] W. Enghardt et al. Nucl. Phys., A 654 (1999) 1047c
[2] R. Hinz, FZ Rossendorf, Wiss.-Tech. Ber. FZR-286 (2000) 59

[1] *Gesellschaft für Schwerionenforschung Darmstadt*

The Influence of the Carbon Ion Beam Microstructure on In-Beam PET Acquisition at GSI Darmstadt: Time-Correlation Measurements [B,G]

K. Parodi, W. Enghardt, J. Pawelke, H. Eickhoff[1], P. Forck[1], T. Haberer[1], D. Schardt[1]

The data registered by the in-beam positron camera for PET quality assurance of ^{12}C ion therapy during particle extraction from the synchrotron are corrupted by a high noise level. Hence, they are rejected before tomographic reconstruction. This reduces the counting statistics of the PET images by a factor of about 2. As a basis for the elaboration of a data acquisition scheme that will avoid this, the physical reason for this increase of noise is under investigation. Previous studies suggested the possible explanation to be a wrong correction of the PET data for random coincidences [1]. The random correction algorithm implemented by the manufacturer of the PET data acquisition system (CTI PET Systems, Knoxville, TN, USA) assumes a slowly varying activity as it is usual in radiotracer imaging. Therefore, the randoms are estimated from the count rate in a delayed coincidence time window shifted by 128 ns with respect to the prompt one. However, if the γ-radiation following nuclear reactions caused by the carbon beam has a microstructure as indicated by [1], this random correction will fail. To test this conjecture, time spectra of the γ-rays following the ^{12}C bombardment of organic matter relative to the synchrotron radiofrequency (RF) have been measured. Being impossible to operate the PET camera for such an investigation, a GSO scintillating crystal coupled to a fast PMT was chosen. GSO exhibits stopping properties very similar to the BGO-detectors of the positron camera but has a 5 times shorter fluorescence time constant and is, therefore, more suited for timing measurements. The size of the GSO-crystal (2 cm radius, 2.5 cm depth) was chosen in order to have a detection efficiency very similar to that of a single BGO block detector of the PET scanner. The electronics scheme is shown in Fig. 1.

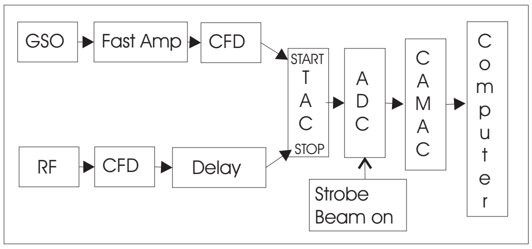

Fig. 1 *Scheme of the NIM-CAMAC electronics used for measuring RF-γ time-distributions.*

The data have been acquired exclusively during particle extraction (beam on). The detector was placed perpendicularly to the beam at the same distance (41 cm) of the PET camera heads from the isocentre of the treatment unit. Five monoenergetic carbon ion beams from 88.83 to 426.11 $AMeV$ with corresponding intensity from $1.5{\cdot}10^8$ to $4 \cdot 10^6$ ions per 2 s spill, resulting in $20-25\%$ ADC dead-time, were completely stopped in blocks of PMMA ($C_5H_8O_2$). This configuration well resembles the typical irradiation conditions during therapy. The experiment confirmed a time-correlation of the detected γ-rays with the synchrotron RF, as shown for the 280.48 $AMeV$ beam in Fig. 2. The shape of the measured time-curve supports the physical hypothesis of [1] that the time distribution of the γ-rays follows the beam microstructure. The steep leading edge of the peak in Fig. 2 is formed by prompt γ-rays following nuclear reactions, whereas the slope of the falling edge is diminished by delayed γ-rays from the decay of isomeric states and radioisotopes with half-lives in the nanosecond region. The constant bias is primarily due to the decay of long-lived isotopes.

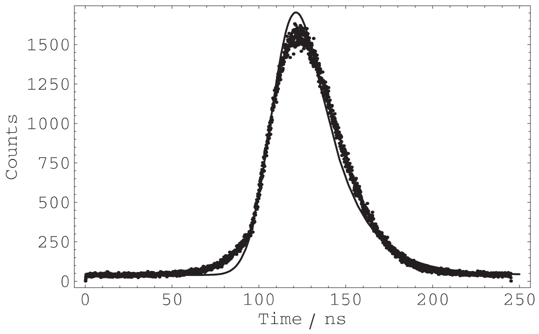

Fig. 2 *Time distribution measured for a 280.48 $AMeV$ ^{12}C beam (RF period: 282.4 ns). The line shows a non-linear least-squares fit based on the model explained in the text.*

This interpretation is obviously supported by a simple model that describes the count rate $N(t)$ by a convolution of the Gaussian beam microbunches with an exponential decay:

$$N(t) = b + a \int_0^t e^{-\frac{(t'-t_0)^2}{2\sigma^2}} e^{-\frac{(t-t')}{\tau}} dt'. \qquad (1)$$

The four free parameters b, a, t_0 and τ are the bias, the normalization, the Gaussian mean value (dependent on the delay of Fig. 1) and an "effective" decay time for all the excited nuclear levels and radioisotopes, respectively. The quantity σ is obtained from the measured FWHM of the beam microstructure [1]. An average value of about 22 ns for the effective decay time was extracted from all the data. Singles energy spectra taken in the same experimental configuration showed a significant amount of events in the γ-ray energy window accepted by the PET camera (250 - 850 keV). This result strongly supports our hypothesis on the nature of the increased noise in the PET data. However, it has to be finally confirmed by a simultaneous energy-time measurement.

[1] K. Parodi et al., FZ Rossendorf, Wiss.-Tech. Ber. FZR-319 (2001) 97

[1] *Gesellschaft für Schwerionenforschung Darmstadt*

A New Fully 3D Maximum Likelihood PET Reconstruction Applicable to Different Detector Arrangements

P. Crespo[1], K. Lauckner[2], W. Enghardt

We developed a fully 3D, maximum likelihood based, PET reconstruction routine applicable to different coincidence detector arrangements for PET. It allows to study the influence of several γ-ray detector geometries onto the corresponding reconstructed images. The scope of this study is to optimize a tomograph to be fully dedicated to the PET monitoring of heavy ion tumor therapy with a rotating beam delivery (gantry).

A special purpose routine was needed in order to surpass situations not approached before: (i) the low counting statistics acquired during therapy with carbon ions makes the application of already developed 3D iterative algorithms with 2D sampling modes impossible, (ii) a fixed dual head PET scanner provides a coincidence detector with spatially variant response, which forbids the application of the algebraic reconstruction methods used in nuclear medicine and (iii) for the unprecedent huge size of coincident channels both for a closed ring camera, or a dual head camera with a small gap, the direct application of the routine previously developed for the positron tomograph at the GSI treatment site [1] is not feasible (the number of possible coincidence channels increases from 4 to 170 millions).

The new routine first samples the list mode data into coincidence channels according to a self-developed channel factorizing scheme. This scheme, combined with direct memory allocation during runtime, feeds the rest of the reconstruction routine with a packed matrix $\boldsymbol{Y}$ containing only the measured data (no empty coincidence channels). The routine than processes $\boldsymbol{Y}$ to find the most probable image $\boldsymbol{X}$ with the maximum likelihood estimation maximization algorithm [2]:

$$x_i^{(n)} = x_i^{(n-1)} \sum_j a_{ij} \frac{y_j}{\sum_k a_{kj} x_k^{(n-1)}} \qquad (1)$$

where $x_i^{(n)}$ is the calculated activity of the i^{th} voxel, at the n^{th} iteration. Each image voxel i contributes with weight a_{ij} to the j^{th} coincidence channel. y_j is the measured activity at the j^{th} channel of the tomograph.

In order to assess the reliability of the new routine we developed a package being capable of simulating PET list mode data sets for a full ring or dual head positron camera. The detector dimensions and positioning are those of the commercial scanner CTI ECAT EXACT HR+ ($\sim$82 cm diameter, $\sim$16 cm axial length). Fig. 1 illustrates a dual head camera with the reference system implemented. Whether implemented on an horizontal beam line or under a rotating gantry, the beam will lie in the plane XZ_{PET} in all situations, as detailed in [3].

Fig. 2 shows a reconstructed image obtained from the simulation of 100 millions annihilation points homogeneously distributed through a hollow sphere with 3 cm outer radius and 1.5 cm inner radius and detected in a closed ring camera. This volume shape was chosen due to its similarity to β^+-distributions that, in radiotherapeutic situations, often occur surrounding the nasal and paranasal cavities of the treated patients with skull base tumours. For this volume shape the geometrical efficiency was 16.2 %. The image shows symmetric, steep edges, corresponding to the simulation.

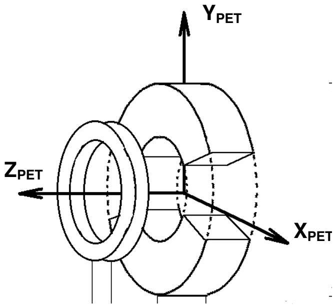

Fig. 1 *Dual head positron camera and metal support ring. The camera rotates around the Z_{PET} axis.*

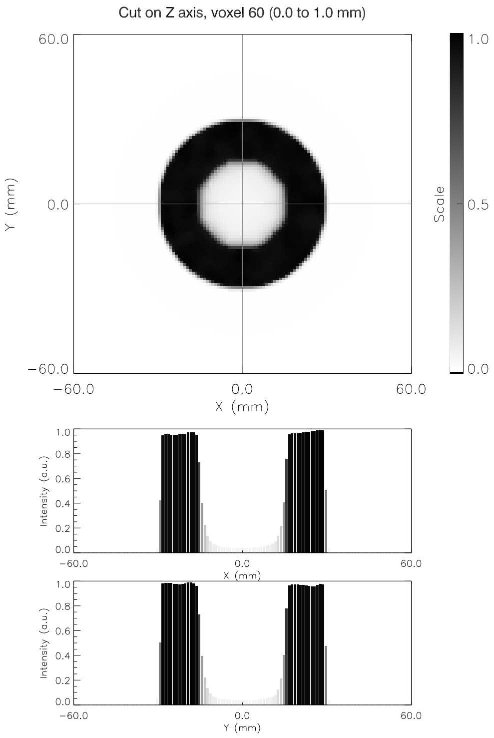

Fig. 2 *Upper image: Reconstructed image (50 iterations) of a simulated hollow sphere. A closed ring PET camera (CTI ECAT EXACT HR+) was simulated, with 16 millions events detected. Axes according to Fig. 1. Lower images: Linear profiles through the axes of the 2D image above.*

[1] *Gesellschaft für Schwerionenforschung Darmstadt*
[2] *The Scientific Consulting Group, Freiburg, Germany*

Fig. 3 illustrates the image degradation induced by the separation of the detectors in a dual head PET camera. The strongest effect seen is the elongation and decrease of intensity of the image along the Y axis. This expected effect arises from the lack of detectors covering that axis in the case of the dual head cameras. Yet, as pointed out, the beam line lies in all situations within the XZ_{PET} plane, where the images do not show the slightest distortion (due to the fact that this plane is perpendicular and symmetric to the gap). This means that the PET quality control of heavy ion radiotherapy is, and can continue to be in the presence of a rotating gantry, extremely precise in the monitoring of the beam range and detection of over-ranges (spikes), mostly in regions located near the iso-center. Lateral straggling evaluation is equally precise in the same terms. The verification of organs at risk lying in planes along the gap (Y_{PET}) would strongly benefit from a PET camera with the smallest possible distance between the heads, if a closed ring is not viable.

The influence of the poor statistics data sets collected in in-beam PET can be seen by comparing the top left image in Fig. 3 and the top image in Fig. 2 (100 times more events). The contours are still clear in the low statistics case, but the images become noisier.

Fig. 4 displays the same situations of Fig. 3 but with twice the number of annihilations simulated, with the result that the image contrast sharpens in all cases.

In summary, a dual head positron tomograph brings the advantage of better flexibility in patient positioning at the expense of loss of intensity and irrecoverable image deformation. These losses can now be quantified with the present routine in order to find an optimum compromise. Still, in order to be able to evaluate the quality of the images from the several camera configurations in real therapeutic situations, β^+-distributions simulated from real treatments [4] should now be interfaced to the reconstruction routine.

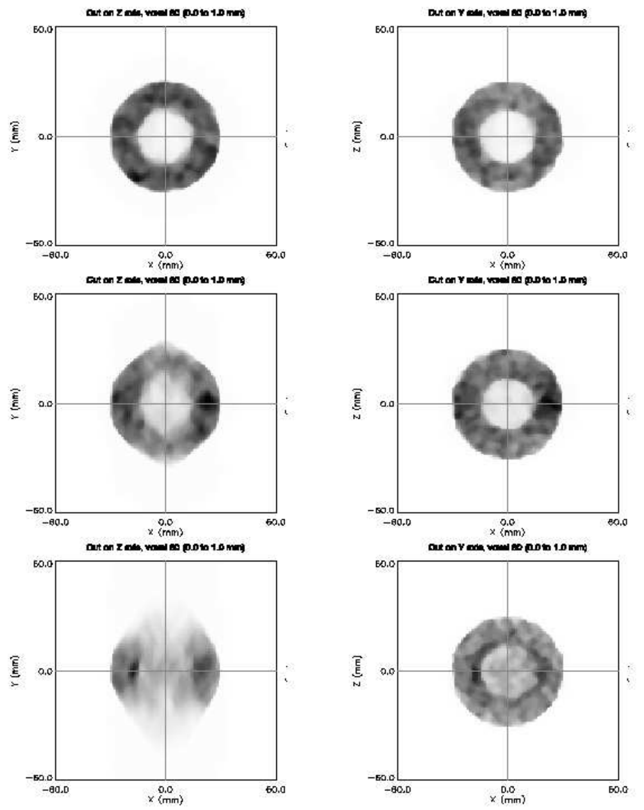

Fig. 3 *Set of images corresponding to the reconstruction (50 iterations) of simulated events detected with a full ring PET camera (top row, 162000 events), a dual head camera with a gap of 34 cm (middle row, 114000 events) and with a gap of 63 cm (bottom row, 69000 events). All simulations followed 1 million annihilations.*

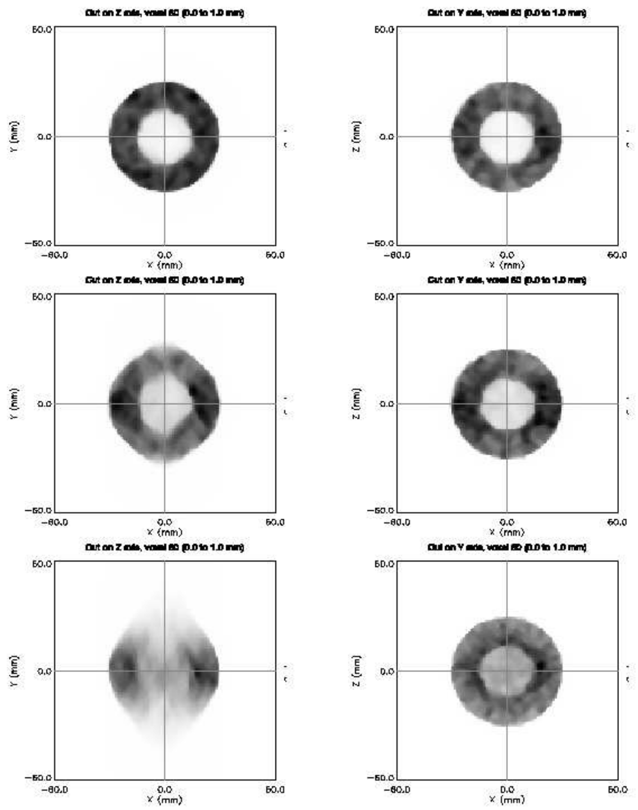

Fig. 4 *Reconstruction details as in Fig. 4, but with 2 times the number of simulated events (2 millions annihilations followed inside the hollow sphere).*

[1] K. Lauckner, FZ Rossendorf, Wiss.-Tech. Ber. FZR-264 (1999)

[2] L.A. Shepp and Y. Vardi, IEEE Trans. Med. Imag. MI-1 (1982) 689

[3] P. Crespo, K. Lauckner, W. Enghardt, FZ Rossendorf, Wiss.-Tech. Ber. FZR-319 (2001) 100

[4] B.G. Hasch, Ph.D. Thesis, Dresden University of Technology (1996)

Evaluation of Avalanche Photodiode Arrays for the Readout of High Granularity Scintillator Matrices

P. Crespo[1], M. Kapusta[2], M. Moszyński[2], W. Enghardt, J. Pawelke, M. Szawlowski[3]

In order to provide sufficient flexibility for patient positioning at the Heidelberg charged hadron tumor treatment facility, γ-ray detectors with large sensitive area and small volume are highly desirable for the positron camera to combine with a rotating beam delivery (gantry). Photon detector technology yields increasingly more compact PET-detectors consisting of inorganic scintillators, e.g. bismuth germanate (BGO) or lutetium oxyorthosilicate (LSO), coupled to either a position sensitive photomultiplier (PSPMT) [1] or to avalanche photodiode arrays (APDAs) [2,3]. We have shown [4] that LSO is a suitable scintillation material for in-beam PET due to its higher light yield and shorter decay time when compared to BGO. APDs are preferable to PMTs due to their higher compactness. Furthermore, the presence of weak stray fields originating from the bending magnets of the gantry may permanently deteriorate the performance of a PSPMT. Therefore, PET-detectors assembled from LSO-crystals and APDA are the first choice for an in-beam positron camera.

With this goal set, we have evaluated the performance of a recently released large area avalanche photodiode (LAAPD) array from Advanced Photonics, Inc. (API). The device is a monolithic 2×2 squared pixels structure with 21 mm^2 total active area and 2.3 mm pitch. Although it presents a high linear fill factor of 90 %, measured in dc-mode with a laser fine scan by the manufacturer, we measured light pulse crosstalk values less than 1.7 % between all pixels by sequentially illuminating the center of one pixel with a 1.7 mm diameter light spot and registering the amplitude spectra of all pixels. These good results are due to the fabrication technique used: one single substrate consisting of a p-type epitaxial layer and an n-type neutron transmutation doped layer is etched using deep reactive ion etching, yielding four adjacent diodes with high gain uniformity. We measured an inter-pixel gain variation with X-rays smaller than 1.3 %. Although the APDA allows stable operation with high gains up to 200, we obtained its noise minimum at an excellent low equivalent noise charge of 16 electrons rms with an internal gain of 50 and with 1 μs signal shaping time.

A 2×2 LSO crystal matrix ($2 \times 2 \times 10\,\mathrm{mm}^3$ each crystal) optically isolated with teflon tape and coupled with silicon oil to the APDA allowed individual crystal identification to be performed, as summarized in Fig. 1. An energy resolution of 12.3 % was obtained for the FWHM of the 511 keV photopeak, a promising result when compared to the ~ 20 % offered by the BGO/PMT solution. The LSO crystals light yield was calibrated with a XP2020Q PMT which allowed the number of electron-hole pairs (e-h) of the APD to be found at 9200 e-h/MeV. Coincidence timing between one LSO/APD channel and a fast scintillator (BaF_2) coupled to a fast PMT resulted in a time resolution of 1.9 ns FWHM, as detailed in Fig. 2. This result is one of the best published for APDAs and corresponds to 2.7 ns FWHM if two LSO/APD detectors are used. Energy and time resolution are essential variables for PET in order to effectively suppress Compton scattered and random events, respectively.

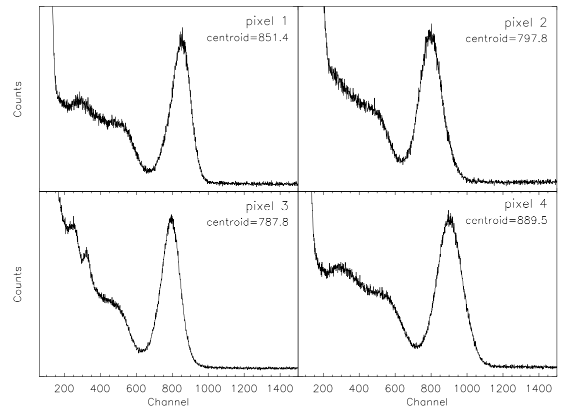

Fig. 1 *Energy spectra from a ^{22}Na γ-source irradiating a 2×2 LSO crystal matrix coupled individually to the 2×2 pixels of the API device.*

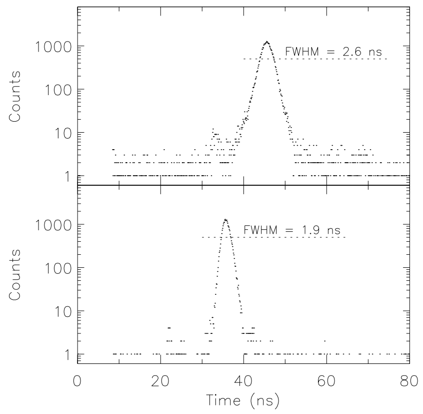

Fig. 2 *Time spectra measured with a ^{22}Na source. Upper image: Threshold set at 350 keV. Lower image: Energy window set at the 511 keV photopeak with a fast-slow setup.*

[1] H. Kyushima et al., IEEE Nucl. Sci. Symp. and Med. Imag. Conf., Lyon (2000), Conference Records
[2] M. Kapusta et al., IEEE Nucl. Sci. Symp. and Med. Imag. Conf., San Diego (2001), Conference Records
[3] S.I. Ziegler et al., Eur. J. Nucl. Med. 28 (2001) 136
[4] K. Lauckner et al., IEEE Nucl. Sci. Symp. and Med. Imag. Conf., Lyon (2000), Conference Records

[1] *Gesellschaft für Schwerionenforschung Darmstadt*
[2] *Soltan Institut for Nuclear Studies, 05-400 Świerk-Otwock, Poland*
[3] *Advanced Photonix, Inc., Camarillo, CA 93012, USA*